Pergamon

*Int. J. Solids Structures* Vol. 31, No. 11, pp. 1493–1517, 1994

0020–7683/94 $7.00 + .00

0020–7683(94)E0014–M

# ANALYSIS OF SHEAR BAND PROPAGATION IN AMORPHOUS GLASSY POLYMERS

P. D. Wu and E. van der Giessen
Laboratory for Engineering Mechanics, Faculty of Mechanical Engineering and Marine Technology, Delft University of Technology, The Netherlands

(*Received* 21 *September* 1993; *in revised form* 15 *January* 1994)

**Abstract**—Similar to the well-known neck propagation phenomenon, shearing of polymer materials often reveals the initiation and subsequent propagation of a shear band. Finite element analysis is used to numerically simulate large plane strain, simple shear tests, focussing attention on the initiation and propagation of the shear band. The mesh sensitivity and effects of initial imperfection, strain softening, orientation hardening, strain-rate as well as the edge effects are discussed in detail. It appears that the intrinsic softening is the driving force to promote initiation of the shear band and its propagation in the shear direction, while the orientation hardening is the driving force for widening of the shear band. The predicted numerical results are compared with experimental data for polycarbonate found in the literature.

## 1. INTRODUCTION

Localization instabilities in the form of shear bands appear to be almost inevitable when a ductile solid undergoes large plastic flow. Such plastic instabilities have a dual significance; as a precursor to fracture and as a mechanism for further deformation. Developing the ability to predict their onset, evolution and subsequent failure is essential for the control of a variety of manufacturing processes and for the design of material microstructures.

The shear localization phenomenon has been widely studied since the early 1970s, primarily for metals (the proceedings edited by Zbib *et al.*, 1992, gives a state-of-the-art overview). It is well-known that localization of plastic flow is strongly directionally sensitive and, therefore, is severely influenced by the evolution of hardening anisotropy that develops with large plastic strains (Rice, 1977). Examples of anisotropic hardening include slip system hardening in metallic single crystals, and the strain-induced molecular orientational hardening that occurs during the drawing of polymers. Commonly, anisotropic hardening has a first-order effect on prediction of localization when compared to an isotropic analysis. More precise and quantitative predictions of localization therefore require improved descriptions of evolving anisotropy.

Although advances in the understanding of plastic instabilities appear to come primarily from researches on polycrystalline metals and solids, a number of characteristic aspects of localization instabilities in polymers begin to be assessed (see e.g. Bowden, 1973; G'Sell, 1986). It is now widely acknowledged that glassy polymers exhibit plastic deformation below the glass transition temperature mainly through the activation of microscopic shear bands. Macroscopic strain localization in polymers can be very different from that in metals due to the dramatic stiffening of polymers at large strains, which is associated with molecular chains orienting and stretching during the deformation process. While plastic instabilities like necks or shear bands in metals almost invariably tend to localize progressively until failure intervenes, necks and macroscopic shear bands in polymers typically do not continue to localize but tend to propagate along the specimen (see e.g. G'Sell *et al.*, 1983; Neale and Tugcu, 1985; Buisson and Ravi-Chandar, 1990). The propagation of localized deformation is fundamental to the processing of polymers since the permanently oriented state generally has enhanced properties, but can also affect subsequent failure. However, the quantitative understanding of thermal-viscoplastic localizations in polymers is still in its infancy. In part, this is due to the fact that appropriate constitutive equations

have been developed only fairly recently. In this study, we focus on a particular type of macroscopic shear localization in amorphous glassy polymers.

Experiments carried out by G'Sell and co-workers have shown that shear band propagation may indeed occur during simple shear of an amorphous polymer such as polycarbonate (e.g. G'Sell and Gopez, 1985). In those experiments, special specimens were used which were designed to create a uniform state of plane simple shear in the gauge section. However, it was found that due to some inhomogeneity in the material, a highly localized shear band appeared near the center of the specimen, which subsequently grew and widened in the direction perpendicular to the shear direction. Grenet and G'Sell (1990) also performed an approximate analysis, using a 1-D constitutive model proposed by G'Sell and Jonas (1979), by means of a simple finite difference method. As a first approximation, they took into account only the shear component of the strain tensor. Recently, Arruda and Boyce (1992) presented a fully 3-D finite element analysis of the test in order to address the effects of edge distortion and material drawn in from the grip sections. Although the predicted nominal shear stress–strain curve was found to accurately capture the observed test data, their analysis did not show the formation of a shear band in the center of the specimen.

In this paper, we first briefly recapitulate the Boyce *et al.* (1988) 3-D constitutive model of large inelastic deformations of amorphous glassy polymers. The yield of initially isotropic glassy polymers has been found to depend on pressure, strain rate, and temperature. After yielding, glassy polymers often strain soften and subsequently strain harden. Adopting a constitutive framework with internal variables, the molecular chain network structure of polymers and its affine deformation attributes particular features to the constitutive formulation. A full network model of rubber elasticity (Wu and van der Giessen, 1992a; 1993a), which is capable of capturing the deformation dependence of hardening, is used to develop a tensorial internal state variable model of evolving anisotropic polymer response. This fully 3-D constitutive model has been found to be able to predict many aspects of the large plastic strain behaviour of glassy polymers observed experimentally (Wu and van der Giessen, 1993a,b,c). In a recent study, a finite element simulation of shear band propagation in glassy polymers was carried out (Wu and van der Giessen, 1992b). In that preliminary study, we considered the simple shear of a polycarbonate specimen of infinite length in the shear direction, based on the fully 3-D constitutive model. Although the problem we solved (Wu and van der Giessen, 1992b) was effectively a 1-D problem across the width of the slab, the results showed that the shear band propagation phenomenon could be, at least qualitatively, captured by the type of constitutive models available at the present moment. However, edge effects could not be taken into account in such a 1-D simulation. Based on detailed experimental observations, G'Sell (1986) suggested that a plane strain type 2-D simulation should be able to reproduce the main features of the experiment. In the present paper, the constitutive model is incorporated in finite element computations of the plane simple shear test, focusing attention on the initiation and propagation of the shear band. Numerical results predicted by the model are compared with experimental results for polycarbonate found in the literature.

Tensors will be denoted by bold-face letters. The tensor product is denoted by $\otimes$ and the following operations for second- and fourth-order tensors apply ($\mathbf{a} = a_{ij}\mathbf{e}_i \otimes \mathbf{e}_j$, $\mathbf{b} = b_{ij}\mathbf{e}_i \otimes \mathbf{e}_j$, $\mathscr{A} = \mathscr{A}_{ijkl}\mathbf{e}_i \otimes \mathbf{e}_j \otimes \mathbf{e}_k \otimes \mathbf{e}_l$, $\mathbf{e}_i$ being a Cartesian basis): $\mathbf{ab} = a_{ik}b_{kj}\mathbf{e}_i \otimes \mathbf{e}_j$, $\mathbf{a}\cdot\mathbf{b} = a_{ij}b_{ij}$ and $\mathscr{A}\mathbf{b} = \mathscr{A}_{ijkl}b_{kl}\mathbf{e}_i \otimes \mathbf{e}_j$. Superscripts T and $-1$ denote the transverse and inverse of a second-order tensor, respectively. The trace is denoted by tr, and a superposed dot denotes the material time derivative or rate.

## 2. CONSTITUTIVE EQUATIONS

The yield of initially isotropic glassy polymers has been found to depend on pressure, strain rate, and temperature. After yielding, glassy polymers often strain soften and subsequently strain harden. Here, we briefly recapitulate the model for large inelastic deformations of glassy polymers developed by Boyce *et al.* (1988), which will be referred to henceforth as the BPA model. The BPA model is developed within an internal variable

framework, but at the same time is to a certain extent based on the micromechanical considerations of the molecular chain network structure of polymers. In the BPA model, the microstructure of an initially isotropic amorphous polymer is assumed to consist primarily of long molecular chains, which are randomly coiled in space. Side groups protrude from the backbone chains at various locations and, in conjunction with overall chain trajectory, can act as nodes, or points of physical entanglement. This results in a network-like structure much like that of rubber, but with the chemical crosslinks replaced by physical entanglements.

Following the pioneering work of Haward and Thackray (1968), it is assumed that a glassy polymer must overcome two physical distinct sources of resistance before large strain inelastic flow may occur. Below the glass transition temperature, prior to initial yield, the material must be stressed to exceed its intermolecular resistance to segment rotation; this will be discussed in Section 2.1. Once the material is free to flow, molecular alignment occurs, resulting in an anisotropic internal resistance to further inelastic deformation, which is called orientational hardening; this will be discussed in Section 2.2.

### 2.1. *Intermolecular resistance*

The intermolecular resistance to plastic flow is considered to be due to the impedance imposed by neighbouring chains on the ability of a chain segment to rotate either individually or in a cluster. Based upon the assumption that plastic flow under an applied shear stress $\tau$ occurs by double-kinking of molecular chains, Argon (1973) developed the following expression for the resulting plastic shear strain rate $\dot{\gamma}^p$:

$$\dot{\gamma}^p = \dot{\gamma}_0 \exp\left[-\frac{As_0}{T}\left(1-\left(\frac{\tau}{s_0}\right)^{5/6}\right)\right]. \tag{1}$$

Here, $\dot{\gamma}$ is a pre-exponential factor, $A$ is a material parameter that is proportional to the activation volume/Boltzmann's constant, $T$ is the absolute temperature and $s_0$ is the athermal shear strength, which in Argon's model is given by $s_0 = 0.077\mu/(1-\nu)$ in terms of the elastic shear modulus $\mu$ and Poisson's ratio $\nu$. Boyce *et al.* (1988) extended this expression to include the effect of pressure and strain softening. They used $s+\alpha p$ instead of $s_0$, where $p$ is the pressure and $\alpha$ is a pressure dependence coefficient. Furthermore, $s$ is assumed to evolve with plastic straining via

$$\dot{s} = h(1-s/s_{ss})\dot{\gamma}^p \tag{2}$$

where $h$ is the rate of resistance drop with respect to the plastic strain and $s_{ss}$ is the assumed saturation value of $s$. The incorporation of this expression (1) into a 3-D constitutive model for rate-dependent plastic flow was also proposed by Boyce *et al.* (1988); for completeness, we give a brief recapitulation in Section 2.3.

### 2.2. *Anisotropic internal resistance*

Once the material is stressed to the point of overcoming intermolecular barriers to chain motion, the molecular chains will tend to align along the direction of principal plastic stretch (see e.g. Haward and Thackray, 1968; Argon, 1973). This action decreases the configurational entropy of the system which, in turn, creates an internal network stress. This process of network distortion is very similar to that of rubber network, and Haward and Thackray (1968) suggested to describe this for uniaxial extension by means of a back stress determined through a Langevin spring, as suggested by non-Guassian network theory. Boyce *et al.* (1988) extended this approach to general 3-D plastic deformations by introducing a back stress tensor $\mathbf{B}$ which is taken to be coaxial with the plastic left stretch tensor $\mathbf{V}^p$ (the precise definition of $\mathbf{V}^p$ will be given in Section 2.3). Thus, if $\mathbf{e}_i^p$ are the unit eigen vectors of $\mathbf{V}^p$, corresponding to a plastic stretch $\lambda_i^p$, the back stress $\mathbf{B}$ is constructed as

$$\mathbf{B} = \sum_i B_i(\mathbf{e}_i^{\mathrm{p}} \otimes \mathbf{e}_i^{\mathrm{p}}) \tag{3}$$

from the principal components $B_i$. Originally, Boyce *et al.* (1988) adopted the classical so-called three-chain model for which the principal components $B_i^{3-\mathrm{ch}}$ of the back stress tensor are given in terms of the plastic stretches $\lambda_i^{\mathrm{p}}$ by (Wang and Guth, 1952)

$$B_i^{3-\mathrm{ch}} = \tfrac{1}{3} C^{\mathrm{R}} \sqrt{N} \left[ \lambda_i^{\mathrm{p}} \mathscr{L}^{-1}\left(\frac{\lambda_i^{\mathrm{p}}}{\sqrt{N}}\right) - \frac{1}{3} \sum_{j=1}^{3} \lambda_j^{\mathrm{p}} \mathscr{L}^{-1}\left(\frac{\lambda_j^{\mathrm{p}}}{\sqrt{N}}\right) \right] \quad (\text{no sum over } i), \tag{4}$$

where $C^{\mathrm{R}}$ is known as the rubbery modulus, $N$ is a statistical network parameter related to the network locking stretch and $\mathscr{L}$ is the Langevin function defined by $\mathscr{L}(\beta) = \coth \beta - 1/\beta$.

More recently however, Arruda and Boyce (1991, 1993) found that the three-chain non-Gaussian network model was not capable of picking up the strain hardening observed experimentally in polycarbonate (PC) and polymethylmetacrylate (PMMA). At the same time they suggested to model the network by eight equivalent chains instead of three and obtained more close agreement with their experimental results for PC and PMMA. The principal components of the back stress tensor according to this eight-chain non-Guassian network model are given by

$$B_i^{8-\mathrm{ch}} = \tfrac{1}{3} C^{\mathrm{R}} \sqrt{N} \mathscr{L}^{-1}\left(\frac{\lambda^{\mathrm{p}}}{\sqrt{N}}\right) \frac{\lambda_i^{\mathrm{p}^2} - \lambda^{\mathrm{p}^2}}{\lambda^{\mathrm{p}}}, \tag{5}$$

where $\lambda^{\mathrm{p}}$ is defined through

$$\lambda^{\mathrm{p}^2} = \frac{1}{3} \sum_{j=1}^{3} \lambda_j^{\mathrm{p}^2}.$$

Both the three-chain and eight-chain model are based on approximate representations of the actual spatial distributions of molecular chains by "lumping" their orientations in three and eight specific directions, respectively. Very recently, the authors developed the so-called full network model in which full account is taken of the 3-D orientation distribution of the individual chains in the network (Wu and van der Giessen, 1992a; 1993a). This model is a 3-D generalization for arbitrary deformation paths of the 2-D model for proportional deformations proposed by Treloar and Riding (1979). The principal back stresses according to this model can be given in two equivalent ways, depending on whether one considers the chain orientation distribution in the undeformed isotropic state or in the current deformed state; here, we only reiterate the expression according to the first point of view because it is more convenient for applications, i.e.

$$B_i = \frac{1}{4\pi} C^{\mathrm{R}} \sqrt{N} \int_0^{\pi} \int_0^{2\pi} \mathscr{L}^{-1}\left(\frac{\lambda^{\mathrm{p}}}{\sqrt{N}}\right) \frac{\lambda_i^{\mathrm{p}^2} m_i^{0^2} - \lambda^{\mathrm{p}^2}/3}{\lambda^{\mathrm{p}}} \sin\theta_0 \, \mathrm{d}\theta_0 \, \mathrm{d}\phi_0 \quad (\text{no sum over } i). \tag{6}$$

Here, $\lambda^{\mathrm{p}}$ is defined by

$$\lambda^{\mathrm{p}^2} = \sum_{j=1}^{3} \lambda_j^{\mathrm{p}^2} m_j^{0^2}$$

and $m_i^0$ are the unit vector components in orientation space defined by

$$m_1^0 = \sin\theta_0 \cos\phi_0,$$
$$m_2^0 = \sin\theta_0 \sin\phi_0,$$
$$m_3^0 = \cos\theta_0,$$

in terms of the angles $\theta_0$ and $\phi_0$ which measure the orientation of molecular chains relative to the principal stretch directions in the undeformed configuration. The numerical evaluation of the integral in (6) is rather time-consuming, but an accurate approximation of the full network predictions according to (6) has been found (Wu and van der Giessen, 1992a) in the form of a combination of the three-chain and eight-chain model predictions (4), (5) through

$$B_i = (1-\rho^p)B_i^{3-ch} + \rho^p B_i^{8-ch}. \tag{7}$$

Excellent agreement with full integration is obtained by taking $\rho^p$ to be related to the maximum principal plastic stretch $\lambda^p_{max} = \max(\lambda^p_1, \lambda^p_2, \lambda^p_3)$ via $\rho^p = 0.85\lambda^p_{max}/\sqrt{N}$. All computations to be reported here have used the expression (7).

### 2.3. *Three-dimensional representation*

Boyce *et al.* (1988) developed the 3-D constitutive relations on the basis of the multiplicative decomposition of the deformation gradient $\mathbf{F}$ into elastic and plastic parts, $\mathbf{F} = \mathbf{F}^e\mathbf{F}^p$. Following Lee (1969) and others, the elastic part $\mathbf{F}^e$ is taken to be symmetric, so that $\mathbf{F}^p$ represents the relaxed configuration obtained by unloading without rotation (in the polar decomposition sense). Hence, $\mathbf{F}^p$ can be decomposed as $\mathbf{F}^p = \mathbf{V}^p\mathbf{R}$ with the plastic stretch $\mathbf{V}^p$ and the total stretch $\mathbf{V}$ in polar decomposition $\mathbf{F} = \mathbf{V}\mathbf{R}$ being related by $\mathbf{V} = \mathbf{F}^e\mathbf{V}^p$. According to this decomposition, the velocity gradient $\mathbf{L}$ is decomposed as

$$\mathbf{L} = \dot{\mathbf{F}}\mathbf{F}^{-1} = \mathbf{D}+\mathbf{W} = \dot{\mathbf{F}}^e\mathbf{F}^{e-1} + \mathbf{F}^e\mathbf{L}^p\mathbf{F}^{e-1}$$

where $\mathbf{D}$ is the rate of deformation, $\mathbf{W}$ is the spin, and $\mathbf{L}^p = \mathbf{D}^p+\mathbf{W}^p = \dot{\mathbf{F}}^p\mathbf{F}^{p-1}$ is the velocity gradient in the relaxed configuration. With the adopted symmetry of $\mathbf{F}^e$, the skewsymmetric part $\mathbf{W}^p$ is algebraically given as $\mathbf{W}$ plus a term dependent on $\mathbf{F}^e$ and $\mathbf{D}+\mathbf{D}^p$ (see Boyce *et al.*, 1988). Since the elastic strains will remain small, we can neglect geometry differences between current and relaxed configurations, $\mathbf{F}^e \approx \mathbf{I}$. When this approximation is carried through consistently, the constitutive equations can be simplified significantly, as discussed by Boyce *et al.* (1988). In particular it is noted that in this case $\mathbf{W}^p \approx \mathbf{W}$ and $\mathbf{D} \approx \mathbf{D}^e+\mathbf{D}^p$, with $\mathbf{D}^e$ the symmetric part of $\dot{\mathbf{F}}^e\mathbf{F}^{e-1}$.

The rate of change of shape of the relaxed configuration, $\mathbf{D}^p$, must be constitutively prescribed. In the BPA model, the magnitude of $\mathbf{D}^p$ is taken to be given by the plastic shear strain rate, $\dot{\gamma}^p$, according to (1) while the tensor direction of $\mathbf{D}^p$ is specified by $\mathbf{N}$, so that

$$\mathbf{D}^p = \dot{\gamma}^p\mathbf{N}, \tag{8}$$

where the direction $\mathbf{N}$ is the deviatoric part of the driving stress, $\tilde{\boldsymbol{\sigma}}'$, normalized by the effective equivalent shear stress $\tau$:

$$\mathbf{N} = \frac{1}{\sqrt{2\tau}}\tilde{\boldsymbol{\sigma}}'$$
$$\tau = \sqrt{\tfrac{1}{2}\tilde{\boldsymbol{\sigma}}'\cdot\tilde{\boldsymbol{\sigma}}'}. \tag{9}$$

Based on the suggestion by Haward and Thackray (1968), the driving stress $\tilde{\boldsymbol{\sigma}}$ itself is defined by

$$\tilde{\boldsymbol{\sigma}} = \boldsymbol{\sigma} - \mathbf{B} \tag{10}$$

where $\boldsymbol{\sigma}$ is the Cauchy stress tensor and $\mathbf{B}$ is the back stress tensor, according to (3) and (6)–(7), due to the strain hardening resulting from molecular alignment, as discussed in Section 2.2. Consistent with the approximation $\mathbf{F}^e \approx \mathbf{I}$, the plastic principal stretches $\lambda^p_i$ to be substituted into (4)–(6) are approximated by the principal values of $\mathbf{V} \approx \mathbf{V}^p$.

In Boyce *et al.* (1988), the Cauchy stress is taken to be given by the elastic constitutive law (Anand, 1979)

$$\boldsymbol{\sigma} = \frac{1}{J}(\mathscr{L}_e \ln \mathbf{F}^e) \tag{11}$$

where $\mathscr{L}_e$ is the fourth-order isotropic elastic modulus tensor:

$$\mathscr{L}_e = \mathscr{L}_e^{ijkl}\mathbf{e}_i \otimes \mathbf{e}_j \otimes \mathbf{e}_k \otimes \mathbf{e}_l,$$

$$\mathscr{L}_e^{ijkl} = \frac{E}{2(1+\nu)}\left[(\delta^{ik}\delta^{jl}+\delta^{il}\delta^{jk}) + \frac{2\nu}{1-2\nu}\delta^{ij}\delta^{kl}\right], \tag{12}$$

with $E = 2(1+\nu)\mu$ being Young's modulus and $J = \det \mathbf{F}^e$. On the basis of these relations, Boyce *et al.* (1988) briefly discuss a possible implementation for the solution of boundary value problems, we here wish to adopt a more typically viscoplastic rate formulation as will be discussed in detail in Section 3. As a consequence, we need the equivalent rate form of the elasticity equations (11)–(12). Since the elastic strains are assumed to remain small, we may replace the hyperelastic law (11) with the hypoelastic rate form

$$\overset{\nabla}{\boldsymbol{\sigma}} = \mathscr{L}_e \mathbf{D}^e \tag{13}$$

in terms of the same modulus tensor $\mathscr{L}_e$ and employing the Jaumann stress rate, $\overset{\nabla}{\boldsymbol{\sigma}} = \dot{\boldsymbol{\sigma}} - \mathbf{W}\boldsymbol{\sigma} + \boldsymbol{\sigma}\mathbf{W}$ to retain objectivity. The constitutive equation (13) can be finally arranged in the following form:

$$\overset{\nabla}{\boldsymbol{\sigma}} = \mathscr{L}_e \mathbf{D} - \dot{\boldsymbol{\sigma}}_v \tag{14}$$

where $\dot{\boldsymbol{\sigma}}_v = \mathscr{L}_e \mathbf{D}^p$ acts as an instantaneous stress rate term that represents the viscoplastic contribution.

## 3. PROBLEM FORMULATION AND METHOD OF SOLUTION

The simple shear deformation of a parallelepiped solid of initial length $2B_0$ and width $2A_0$ can be basically defined, as illustrated in Fig. 1, by the homogeneous relative glide of parallel planes along the shear direction. The amount of shear is commonly expressed by the ratio $\Gamma = U/(2A_0)$, where $U$ is the relative displacement of the opposite faces of the parallelepiped. In order to impose a constant shear rate $\dot{\Gamma} = \dot{U}/(2A_0)$, the opposite faces are displaced at a constant velocity $\dot{U} = \dot{\Gamma}(2A_0)$. Variations of the thickness during the deformation are relevant only to second-order terms in the strain tensor and may be

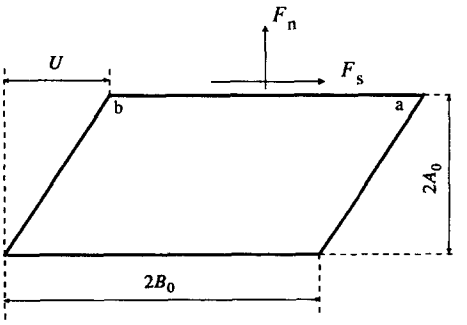


Fig. 1. Schematic definition of the speciman under the plane strain simple shear.

neglected to a first approximation (G'Sell, 1986); thus, this deformation mode is of a 2-D plane strain type. The conventional nominal shear stress and normal stress are defined by $F_s/(2B_0)$ and $F_n/(2B_0)$, respectively, where $F_s$ and $F_n$ are the applied shearing force and the force required to maintain the width of the specimen, respectively.

In the experiments carried out by Gopez (1983) and by G'Sell and Gopez (1985), specimens were used which were designed to create a uniform state of plane simple shear in the gauge section. However it was found that, due to some inhomogeneity in the material, a highly localized shear band appeared near the center of the specimen, which subsequently grew and widened in the direction perpendicular to the shear direction. To trigger the initiation of such a macroscopic shear band at the center of the specimen in our 2-D analysis, we assume here an initial imperfection of the shear strength $s_0$ of the form

$$\Delta s_0 = \xi s_0 \exp\left[-\frac{(x-B_0)^2+(B_0/A_0)^2(y-A_0)^2}{0.01(B_0^2+A_0^2)}\right] \tag{15}$$

such that the initial shear strength is $s_0-\Delta s_0$, where $\xi$ determines the intensity.

A numerical analysis is performed by employing a finite strain finite element scheme in a manner similar to that described by Needleman and Tvergaard (1984), in which a Langrangian formulation is adopted for the governing equations. The initial undeformed configuration of the body with volume $V$ and surface $S$ is chosen as a reference. A material point is identified by the convected coordinates $x^i$ in the reference configuration and with base vectors $\mathbf{g}_i$ and corresponding metric tensor $g_{ij}$, while in the current configuration the base vectors are $\mathbf{G}_i = \mathbf{F}\mathbf{g}_i$ with metric tensor $G_{ij}$. The displacement and velocity components on the reference base vectors are $u^i$ and $v^i$, respectively, and the Langrangian strain tensor components are given by

$$\eta_{ij} = \tfrac{1}{2}(u_{i,j}+u_{j,i}+u^k_{,i}u_{k,j}),$$

where a comma denotes covariant differentiation with respect to the undeformed metric. Note that the $\dot{\eta}_{ij}$ are equal to the covariant Eulerian strain-rate components $D_{ij}$ of $\mathbf{D}$ on the current deformed basis, but that this correspondence does not hold for the respective contravariant components.

The Kirchhoff stress components $\tau^{ij}$ dual to $\eta_{ij}$ are defined in terms of the Cauchy stress components with respect to the deformed base vectors, $\sigma^{ij}$, by

$$\tau^{ij} = (\det \mathbf{F})\sigma^{ij}.$$

The nominal traction vector $\mathbf{T}$ on a surface element is defined with respect to the unit normal $\mathbf{n}$ in the reference configuration and has components

$$T^i = n_j(\tau^{ij}+\tau^{kj}u^i_k).$$

The equations of equilibrium are expressed in terms of the principle of virtual work, which under quasi-static conditions takes the form

$$\int_V \tau^{ij}\,\delta\dot{\eta}_{ij}\,\mathrm{d}V = \int_S T^i\,\delta v_i\,\mathrm{d}S.$$

The conditions for satisfying incremental equilibrium are obtained by expanding the above equation about the current state yielding

$$\int_V (\dot{\sigma}^{ij}\delta D_{ij} + \sigma^{ij} v^k_{,i} \delta v_{k,j})\, \mathrm{d}V = \int_S \dot{T}^i \delta v_i \, \mathrm{d}S. \tag{16}$$

Here we have immediately expressed the relationship in terms of the Cauchy stress rather than the Kirchhoff stress, using the fact that the relative volume change $\det \mathbf{F} - 1$ is entirely due to elastic strains, which remain small. Furthermore, we have substituted $\dot{\eta}_{ij} = D_{ij}$.

When the elastic-viscoplastic constitutive law (14) is substituted into (16), the time-dependent terms $\dot{\sigma}_v$ can be combined with the nodal traction-rate vector. No contribution to the stiffness matrix arises from the variations of plastic deformation rate since these do not explicitly depend on stress rates. We use quadrilateral elements, each built up of four linear velocity, triangular subelements arranged in a "crossed triangle" configuration. An equilibrium correction procedure is employed to avoid drifting away from the true equilibrium path during the incremental procedure. Integrations with respect to time are computed using an explicit Euler integration method. Since the elements of the stiffness matrix are of the order of the elastic moduli, as given by (12), very small time steps have to be employed to achieve satisfactory convergence in the early stages of viscoplastic flow; however, at later stages of well-developed viscoplastic flow, much larger steps may be used. For this reason we use an adaptive time stepping method proposed very recently by van der Giessen and Neale (1993), in which the time step size $\Delta t$ to be used for each increment is determined adaptively through an automatic procedure consisting of three key parts.

Part 1: The first two steps are performed with very small time steps such that any plastic deformation is excluded. The size of the time step is defined as a small fraction of a reference time scale $t_R$,

$$\Delta t = 10^{-8} t_R, \quad t_R = \frac{s_0}{\mu \dot{\gamma}^p}\left[1 + \frac{T}{A s_0} \ln\left(\frac{\dot{\gamma}^p}{\dot{\gamma}_0}\right)\right]^{6/5},$$

which, in a loose sense, relates the viscoplastic shear rate $\dot{\gamma}^p$ according to eqn (1) with the elastic shear rate $\dot{\Gamma}$ under the same stress.

Part 2: At the beginning of the third time step, the time increment is determined on the basis of a prescribed work rate per unit volume, $W = (\dot{F}_s \dot{U} \Delta t)/(4A_0 B_0)$, during that step. The applied work rate is estimated on the basis of the 'elastic' stress state determined as discussed above and $W$ is scaled wth the elastic shear modulus $\mu$, i.e. $W \equiv \varepsilon_W \mu$. Thus, the time increment is obtained from

$$\Delta t = \varepsilon_W \frac{4\mu A_0 B_0}{\dot{F}_s \dot{U}}$$

and its size is controlled by the parameter $\varepsilon_W$.

Part 3: During all subsequent increments, a maximum allowable time step $\Delta t_m$ is determined as the maximum value of $\Delta t'$ computed from each of the following criteria:

$$\Delta t' \leqslant \varepsilon_s \frac{s}{h|1 - s/s_{ss}|\dot{\gamma}^p};$$

$$\Delta t' \leqslant \frac{\Delta \gamma^p_{max}}{\dot{\gamma}^p}. \tag{17}$$

The first criterion ensures that the shear stress drop during a time increment $\Delta t'$ does not exceed a fraction $\varepsilon_s$ of the current shear strength. The second criterion ensures that the plastic shear strain increment during a time increment $\Delta t'$ does not exceed a maximum shear increment $\Delta \gamma^p_{max}$. If at the end of the increment $\Delta t_m$ is smaller than the current time step $\Delta t$, the time step of the next increment is taken equal to $\Delta t_m$; if $\Delta t_m$ exceeds $\Delta t$ for a number of consecutive increments (say, five), $\Delta t$ increased by a factor 1.5.

As pointed out by van der Giessen and Neale (1993), the procedure is rather heuristic, but extremely simple to implement in an incremental code. This adaptive time step selection procedure involves three parameters, the values of which have to be determined empirically. The results to be presented in the next two sections have all been obtained with the following values: $\varepsilon_W = 10^{-8}\,s^{-1}$, $\Delta\gamma^p_{max} = 0.0025$, $\varepsilon_s = 0.01$. These values have been found to ensure numerical stability in all cases to be presented. Several cases have been repeated with half of the above values, and in each case the differences in the global response quantities (shear and normal stresses) remained smaller than 0.1%.

We would like to note that powerful forward gradient approaches for the time integration of viscoplastic constitutive equations have been proposed in the literature (e.g. Peirce *et al.*, 1984). However, these methods are very difficult to apply to the present set of constitutive equations because of the structure of the back stress equations (3)–(7). By employing the afore-mentioned simple adaptive time stepping scheme, we have been quite efficient in obtaining stable solutions with acceptable numbers of increments.

## 4. PARAMETER STUDY

The problem described in Section 3 involves a number of dimensionless groups and therefore we introduce the following nondimensional quantities:

$$\text{loading:}\quad \Gamma = \frac{U}{2A_0},\quad \sigma_s = \frac{F_s}{2B_0 s_0},\quad \sigma_n = \frac{F_n}{2B_0 s_0},\quad \frac{\dot{\Gamma}}{\dot{\gamma}_0}; \tag{18}$$

$$\text{geometry:}\quad B_0/A_0; \tag{19}$$

$$\text{material:}\quad \frac{E}{s_0},\ \frac{s_{ss}}{s_0},\ \frac{As_0}{T},\ \frac{h}{s_0},\ \nu,\ \alpha,\ N,\ \frac{C^R}{s_0}. \tag{20}$$

The overall response of the specimen can be conveniently presented in terms of the applied shear strain $\Gamma$, and the normalized nominal shear stress and normal stress, $\sigma_s$ and $\sigma_n$, respectively.

### 4.1. *A typical result*

Figure 2 shows the predicted response to plane strain simple shear, using a regular mesh with $12 \times 60$ elements (12 equally sized elements in the direction perpendicular to the

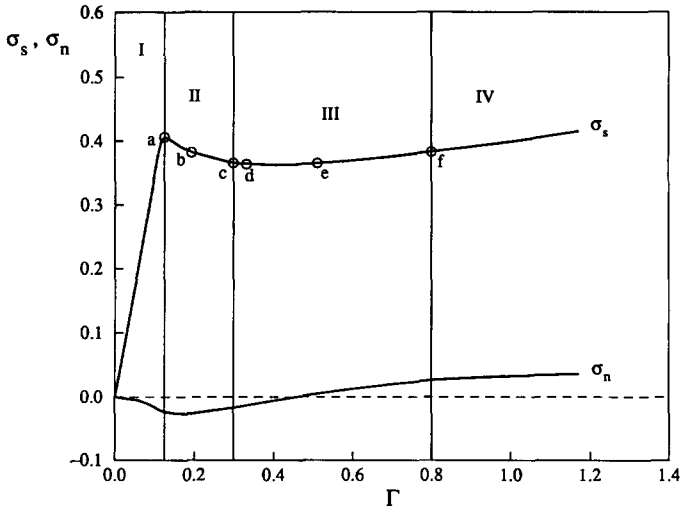


Fig. 2. Typical predicted simple shear behaviour for a specimen with $B_0/A_0 = 15$, $\xi = 0.01$ and for the following values of the material parameters: $\dot{\Gamma}/\dot{\gamma}_0 = 1.5 \times 10^{-18}$; $E/s_0 = 9.38$; $s_{ss}/s_0 = 0.92$; $As_0/T = 79.2$; $h/s_0 = 9.28$; $\nu = 0.3$; $\alpha = 0.08$; $N = 6.3$; $C^R/s_0 = 0.06$. Stages a–f correspond to the plots shown in Fig. 3.

shear direction, 60 in the shear direction). The specimen dimensions are specified by $B_0/A_0 = 15$, and the following values of the material parameters were used: $\dot{\Gamma}/\dot{\gamma}_0 = 1.5 \times 10^{-18}$, $E/s_0 = 9.38$, $s_{ss}/s_0 = 0.92$, $As_0/T = 79.2$, $h/s_0 = 9.28$, $\nu = 0.3$, $\alpha = 0.08$, $N = 6.3$, $C^R/s_0 = 0.06$. These values, except the value $E/s_0$, were primarily used as representative values of the parameters, but are reasonable for polycarbonate among other amorphous glassy polymers. In the BPA model, the value of $E/s_0$ is determined uniquely by Poisson's ratio. However, here we consider it to be an independent material parameter. The reason for this is that the constitutive model described in Section 2 cannot account for the small strain viscoelastic behaviour observed in experiments, resulting in a nonlinear stress–strain response prior to yielding. Now, since we are mainly interested in large plastic deformations, these viscoelastic effects need not be considered in detail, and we shall simply characterize the behaviour prior to yielding by an appropriate value of $E$. The intensity $\xi$ of the initial imperfection [see eqn (15)] is assumed to be 0.01. We will use these values of the parameters throughout Section 4, except where noted otherwise.

The four successive stages of the experimental shear stress-shear strain curve distinguished by G'Sell and Gopez (1985) are picked up qualitatively by the simulation (Fig. 2): (I) the elastic response ending at a yield strain of about 0.12; (II) a small but significant shear stress drop, spreading over a strain range from 0.12 to 0.3; (III) a plastic domain with a very small apparent slope, spreading over a strain range from 0.3 to about 0.8; (IV) large plastic flow of the sample with enhanced hardening. The calculation ended when the maximum plastic stretch approached the locking stretch $\sqrt{N}$ of the macromolecular chain network at some point in the specimen.

Figure 2 also shows the development of the normal stress $\sigma_n$ during simple shear. The compressive normal stress increases up to an applied strain of 0.18, where it approaches its maximum of about 0.027. From that point on, the normal stress starts to increase and increases monotonically towards a constant positive value. The normal stress remains compressive up to an applied strain of about 0.5 and then becomes tensile.

G'Sell and Gopez (1985) showed that the four stages in the shear stress–shear strain behaviour can be partly attributed to the intrinsic material behaviour and partly to the occurrence of a macroscopic shear band. In order to clearly show the initiation and propagation of the shear band, Fig. 3 shows contour plots of the plastic shear strain $\gamma^p$ normalized by the "applied plastic strain"

$$\Gamma^p = \Gamma - F_s/(2B_0\mu),$$

at different stages of the deformation (the stages a–f correspond to the points marked a–f in Fig. 2). As the shear stress passes through its maximum at $\Gamma \approx 0.12$, a region of enhanced shear appears at the location of the initial imperfection [see Fig. 3(a)]. It is noted that in addition, two regions of enhanced shear are found near the free edges. During continued deformation, these regions quickly grow into shear bands: the shear band initiated at the center elongates in the shear direction while the other two propagate towards the center of the specimen [see Fig. 3(b)] until they link up with each other and form a single shear band at around $\Gamma = 0.30$ [see Fig. 3(c)]. Then the so-formed single shear band gradually widens [Figs 3(d,e)]. As observed in experiments, the local plastic shear strain within the shear band continues to increase at a very slow rate during band widening. Figure 3(f) shows the contour plots when the band occupies the whole specimen.

The physical cause for shear band propagation is evident from the evolution of the shear stress. When the band of increased plastic flow is initiated near the center, the local shear stress drops sharply as a consequence of the intrinsic softening. With continued applied shearing, orientation hardening starts to develop in the shear band, causing the neighbouring material to reach the local shear resistance and initiate substantial plasticity. This process continues until most of the specimen is well in the plastic, strain hardening regime.

### 4.2. *Influence of the mesh*

Shear band localization phenomena are notorious for sometimes exhibiting a pathological mesh sensitivity. However, as put forward unequivocally by Needleman (1988), this


Fig. 3. Contours of normalized plastic shear strain $\gamma^p/\Gamma^p$ under simple shear predicted with the $12 \times 60$ mesh at various shears: (a) $\Gamma = 0.12$; (b) $\Gamma = 0.20$; (c) $\Gamma = 0.30$; (d) $\Gamma = 0.33$; (e) $\Gamma = 0.51$; (f) $\Gamma = 0.80$.

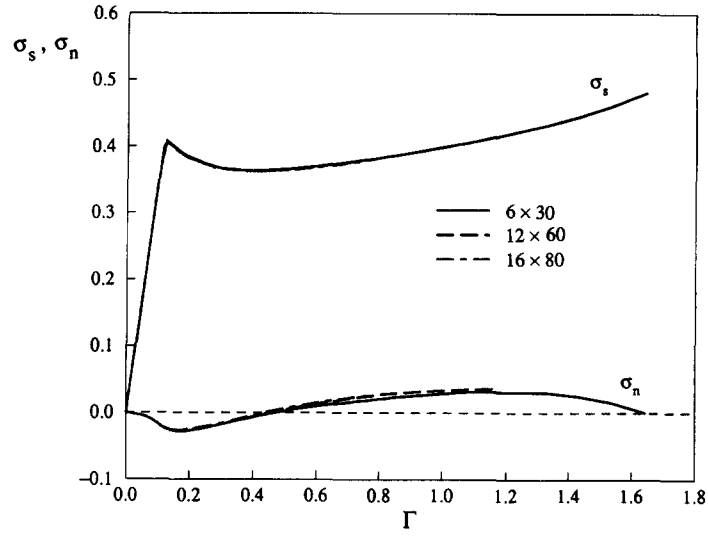


Fig. 4. Shear and normal stress responses under simple shear predicted with different finite element meshes.

is not necessarily the case for the problem under consideration here since the material response according to the constitutive model of Section 2 is intrinsically rate-dependent. Nevertheless, the selection of a proper mesh does require attention. Numerical experiments have shown that the overall response of the specimen, in terms of the overall shear stress and normal stress, are not sensitive to the mesh, but it turned out that details of shear band formation and propagation are indeed rather sensitive to the mesh used. In order to obtain sufficiently accurate results we have to use somewhat fine mesh.

Figure 4 shows the predicted responses to plane strain simple shear using three different regular meshes consisting of $6 \times 30$, $12 \times 60$ and $16 \times 80$ elements. In all these calculations we have used the same parameters as given in Section 4.1.

Figure 5 gives the contour plots of plastic shear strain at various stages of the deformation with the mesh ($16 \times 80$). It is clear that the contour plots with mesh ($16 \times 80$) are almost identical to these with mesh ($12 \times 60$), which have been discussed in detail before. However, when the crude mesh ($6 \times 30$) is used (see Fig. 6), we do not observed the thin shear band at the location of the initial imperfection up to shear strains about 0.3 (stages a and b of Fig. 6). The reason for this is that the width of a shear band at the early stages is very small; if it is smaller than the element size of the mesh, it will not be picked up in the analysis.

Further detailed studies of the distributions of plastic shear strain and stresses reveal that the edge effects are very strong. Indeed, the maximum plastic stretch always approaches the locking stretch of the macromolecular chain network at a location near the edges. On the other hand, the extent of the stress concentration is sensitive to the mesh used. Using a crude mesh tends to reduce the stress concentration. Actually, the most important difference between the crude and the fine meshes in Fig. 4 is that the maximum plastic stretch formed with the fine mesh ($16 \times 80$) approaches the locking stretch at an applied shear strain of about only 0.8, while in the crude mesh ($6 \times 30$) the locking stretch is not reached prior to $\Gamma = 1.6$. Based on all those observations, we decided that the relatively fine mesh ($12 \times 60$) would be sufficiently accurate. We will use this mesh in the rest of this paper, except where noted otherwise.

### 4.3. *Effects of initial imperfection*

To check the influence of the initial imperfection on the localization results, we have used different imperfection shapes and sizes. It was found in all cases that, within the strain-range considered, the overall response is not sensitive to the initial imperfection. In fact, we hardly see the effect of the initial imperfection on the overall response from the predicted

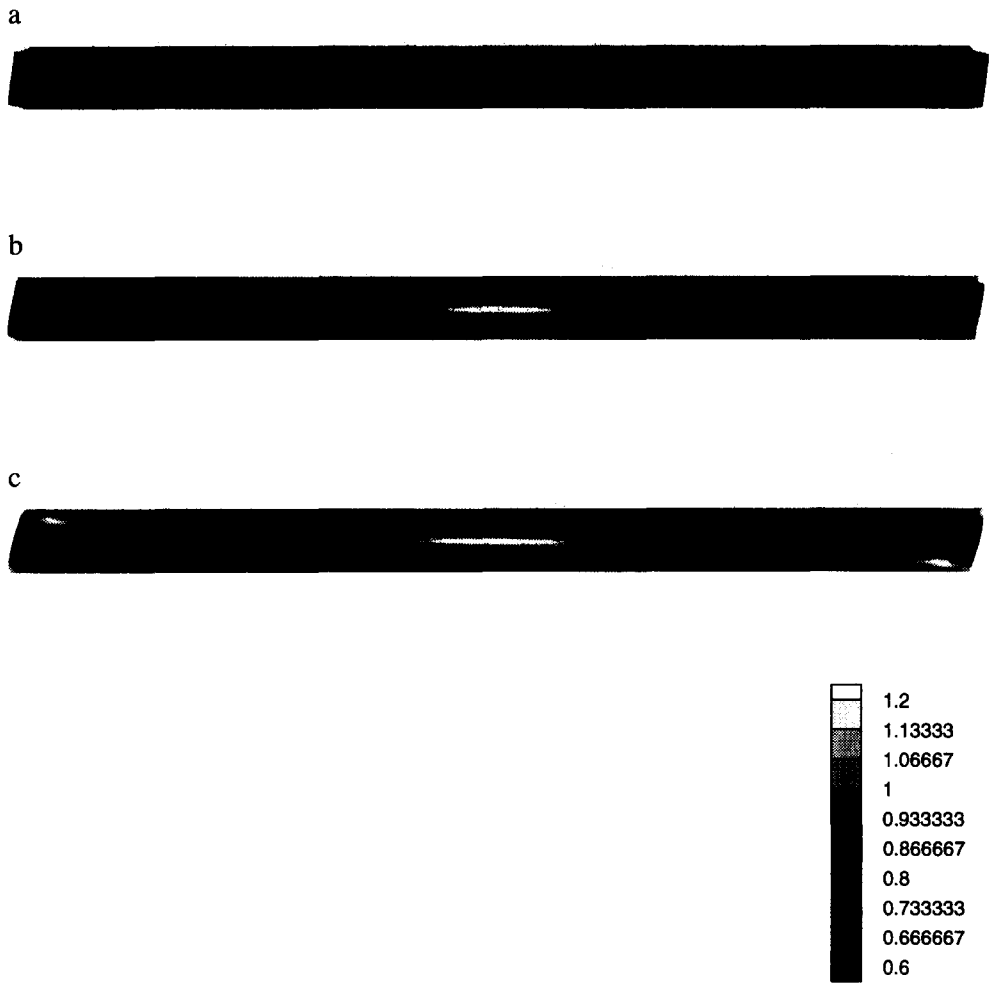


Fig. 5. Contours of normalized plastic shear strain $\gamma^p/\Gamma^p$ for the $16 \times 80$ mesh at various deformation stages: (a) $\Gamma = 0.12$; (b) $\Gamma = 0.20$; (c) $\Gamma = 0.30$.

shear and normal stresses. We have also studied the normalized plastic shear strain distribution by using the same imperfection shape, given by eqn (15), but with different intensities $\xi$ ranging from 0.005 to 0.02: the differences were found to be very small.

Nevertheless, it is interesting to consider the limiting cases of an idealized specimen without initial imperfection ($\xi = 0$). Figure 7 shows the normalized plastic shear strain distribution in this case. As opposed to Fig. 3, there is no shear band initiated at the center of the specimen. However, we do observe the two regions of intense shear near the free edges [Fig. 7(a)], which propagate towards the center of the specimen during softening [see Figs 7(b,c)] until they join each other and form a single shear band at an applied shear strain about 0.33. Then the so-formed shear band gradually widens until it occupies the entire area of the specimen [see Fig. 7(d)]. From that point on, the differences in plastic shear strain distribution between the specimens with and without an initial imperfection are no longer distinguishable.

### 4.4. *Effects of material properties*

It is generally agreed that the yield and postyield behaviour of glassy polymers exhibit true strain softening (see e.g. Haward, 1980). In the BPA model, the effects of softening are described in terms of the evolution equation (2) of the athermal yield strength. We study the effects of softening on shear band initiation and propagation by considering different intensities of softening, by taking $s_{ss}/s_0 = 0.92$ and 0.79, respectively. The associated value of the parameter $h$, the slope of the yield drop with respect to plastic strain, is adjusted

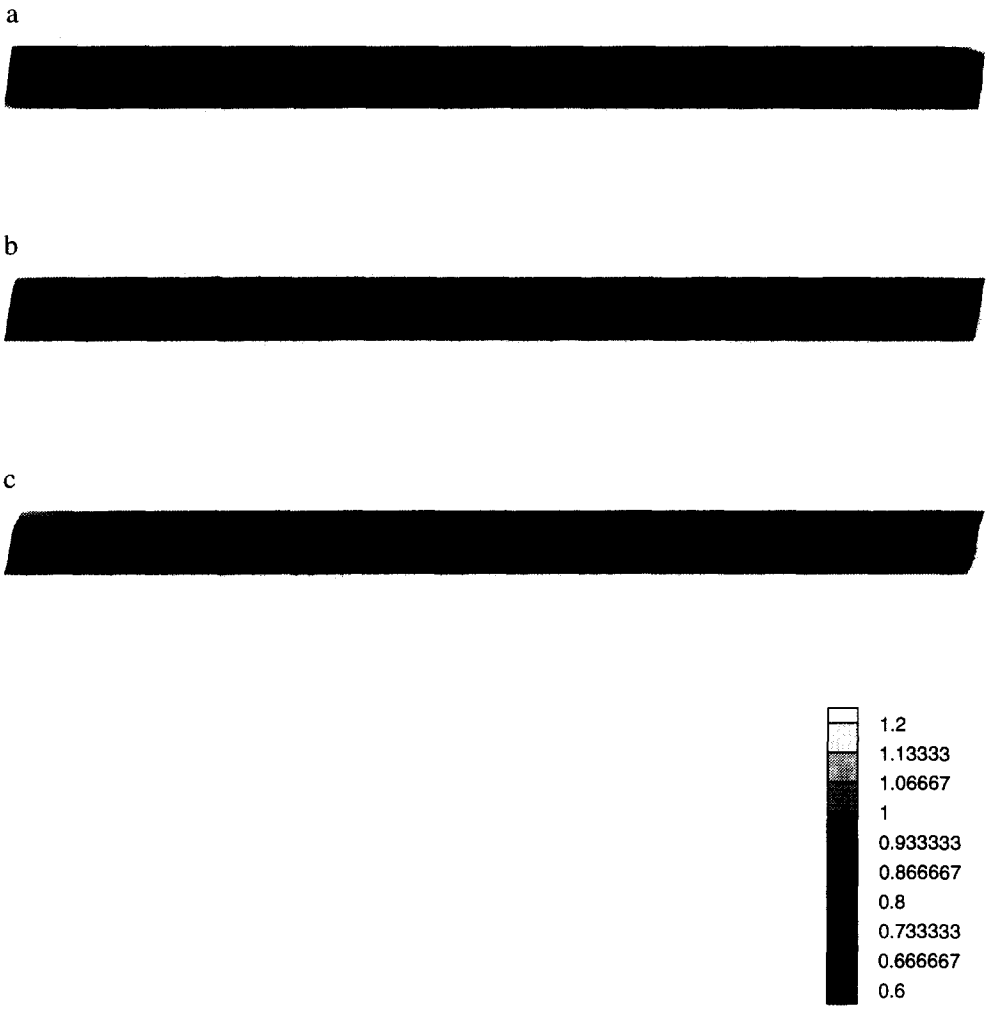


Fig. 6. Contours of normalized plastic shear strain $\gamma^p/\Gamma^p$ for the $6 \times 30$ mesh at various deformation stages: (a) $\Gamma = 0.12$; (b) $\Gamma = 0.20$; (c) $\Gamma = 0.30$.

in such a way that the initial slope of softening, $h|1 - s_0/s_{ss}|$, remains constant. We also include the limiting case of no softening by assuming $s_{ss}/s_0 = 1$.

Figure 8 shows the effects of softening on the predicted shear and normal stress responses. As expected, the parameter $s_{ss}/s_0$ determines the extent of softening. Detailed consideration of the plastic shear strain distributions for the various cases indicates that there is no evidence of initiation and propagation of a shear band in the limiting case of no intrinsic softening. Discussion on the distributions of normalized plastic shear strain predicted with $s_{ss}/s_0 = 0.79$ will be given later.

The parameters $N$ and $C^R$ govern the orientation hardening through the non-Gaussian network model for rubber elasticity (6). Here, we study the effect of orientation hardening by first using the same value of $N$ ($N = 6.3$) but different values of $C^R$: $C^R/s_0 = 0.06$, 0.12 and 0.18, respectively. Furthermore, we include a limiting case of no orientation hardening by taking $C^R/s_0 = 0$. In all these calculations, the intensity of softening is assumed to be $s_{ss}/s_0 = 0.79$. The numerical results are presented in Fig. 9. It is clear from the predicted shear stresses that a larger value of $C^R/s_0$ increases the stiffness of the network and therefore increases the orientation hardening. The value of $C^R/s_0$ is observed to affect the apparent overall yield stress too. The reason for this is that at the yield strain $\Gamma \approx 0.12$, significant plastic deformation has already occurred at some locations due to the intrinsic inhomogeneity of deformation. If $C^R$ is large, orientation hardening would be already significant at that moment, resulting in a noticeable increase of the yield stress. The normal stress

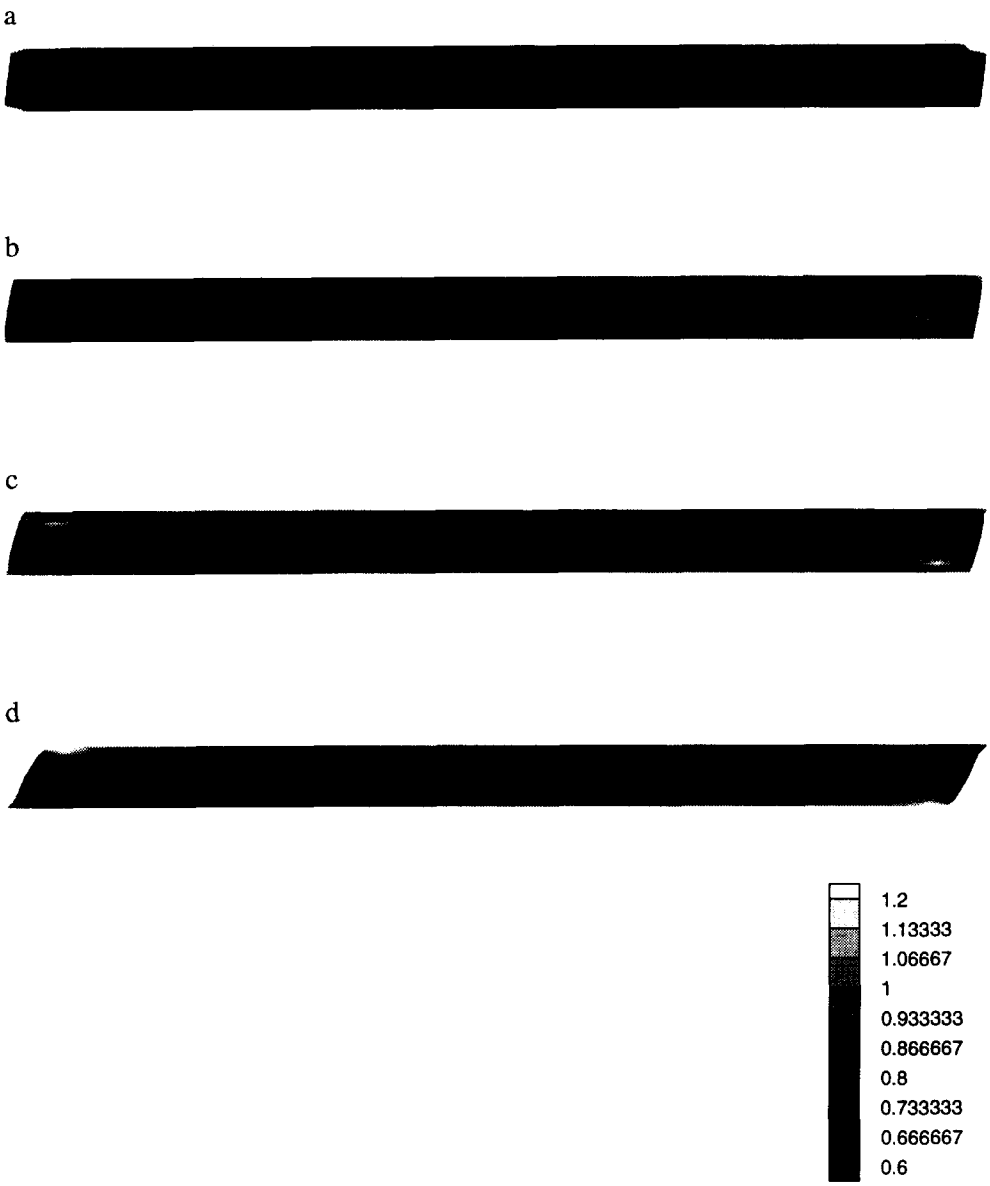


Fig. 7. Contours of normalized plastic shear strain $\gamma^p/\Gamma^p$ in an idealized specimen without an initial imperfection at various deformation stages: (a) $\Gamma = 0.12$; (b) $\Gamma = 0.19$; (c) $\Gamma = 0.30$; (d) $\Gamma = 0.80$.

responses with different values of $C^R/s_0$ give virtually identical predictions up to $\Gamma = 0.2$, where they approach the maximum compressive stress. From that point on, the normal stress for little ($C^R/s_0 = 0.06$) or no hardening ($C^R/s_0 = 0$) increases monotonically and becomes tensile at an applied shear strain of 0.25. As opposed to this result, the normal stress response for larger values of $C^R/s_0$ of 0.12 or 0.18 is not monotonic but reaches a maximum and then drops monotonically again. In the case of $C^R/s_0 = 0.18$ the normal stress response maintains compressive during the entire deformation process.

The distributions of the normalized plastic shear strain predicted with relatively large values of $C^R/s_0$ (0.12 or 0.18) are found to be similar to those shown in Fig. 3. The distributions of normalized plastic shear strain obtained with $C^R/s_0 = 0$ (i.e. no orientation hardening) are given in Fig. 10. We did not observe a shear band at small strains up to $\Gamma \approx 0.16$. During continued deformation, the shear band initiated at the center [see Fig. 10(a)] elongates in the shear direction while the other two, initiated near the free edges, propagate towards the center of the specimen [see Fig. 10(b)] until they link up each other and form a single shear band [see Fig. 10(c)]. It is found that the so-formed shear band does not widen as we observed in the cases with a positive value of $C^R/s_0$, but localizes with further

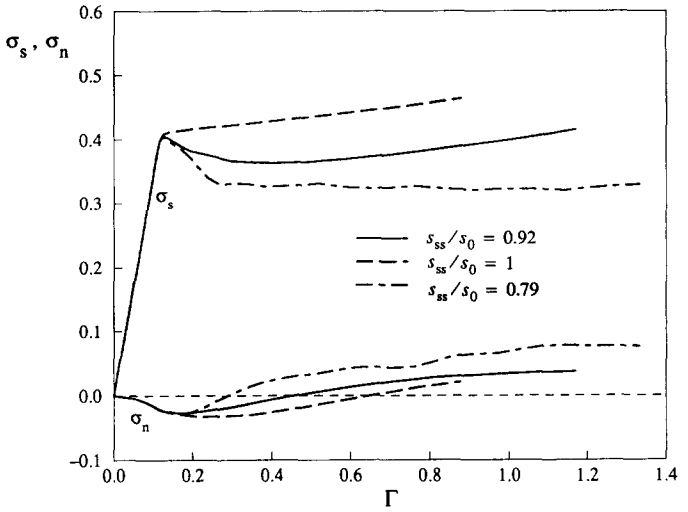


Fig. 8. Influence of the softening parameter $s_{ss}/s_0$ on the predicted shear and normal stress responses under simple shear. All other parameters are as in Fig. 2.

shearing [Figs 10(d,e)]. The strain is concentrated in the shear band, as is seen from the profiles of the specimen in Figs 10(d,e), while strains outside the band remain almost constant or even slightly decrease. This is also the reason why the predicted shear stress continues to decrease at large strains, as shown in Fig. 9. Eventually, the maximum plastic shear strain approaches the limit value $\sqrt{N}$ at the surface of the shear band near the center of the specimen. In the case of small orientation hardening ($C^R/s_0 = 0.06$), the shear band is found to widen but very slowly.

We proceed by studying the effects of orientation hardening by using the same value of $C^R$ ($C^R/s_0 = 0.06$) but different values of $N$: $N = 3.0$, 6.3 and 9.0. The results are presented in Fig. 11. The effects of $N$ on the overall response of the simple shear test are not very strong, except for the fact that the limit stretches are being reached at different strain levels.

Flow in amorphous glassy polymers appears to be a viscous process and the yield stress is strongly strain-rate dependent. Figure 12 shows the overall responses to simple

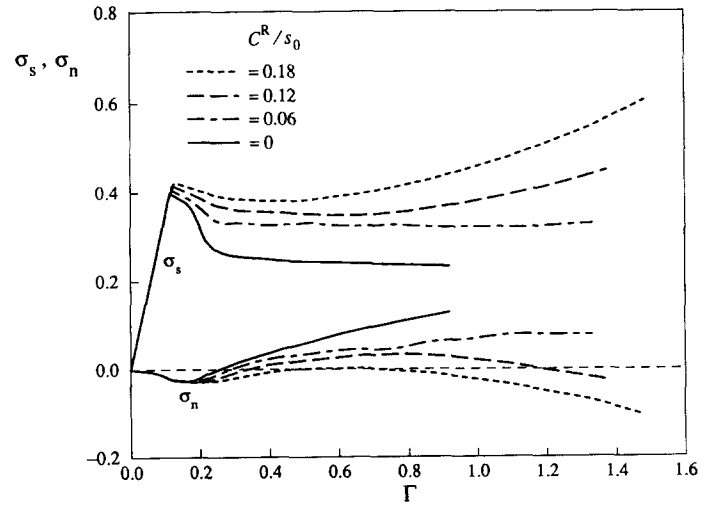


Fig. 9. Influence of the orientation hardening parameter $C^R/s_0$ on the predicted shear and normal stress responses under simple shear. Softening is characterized by $s_{ss}/s_0 = 0.79$ and all other parameters are as in Fig. 2.

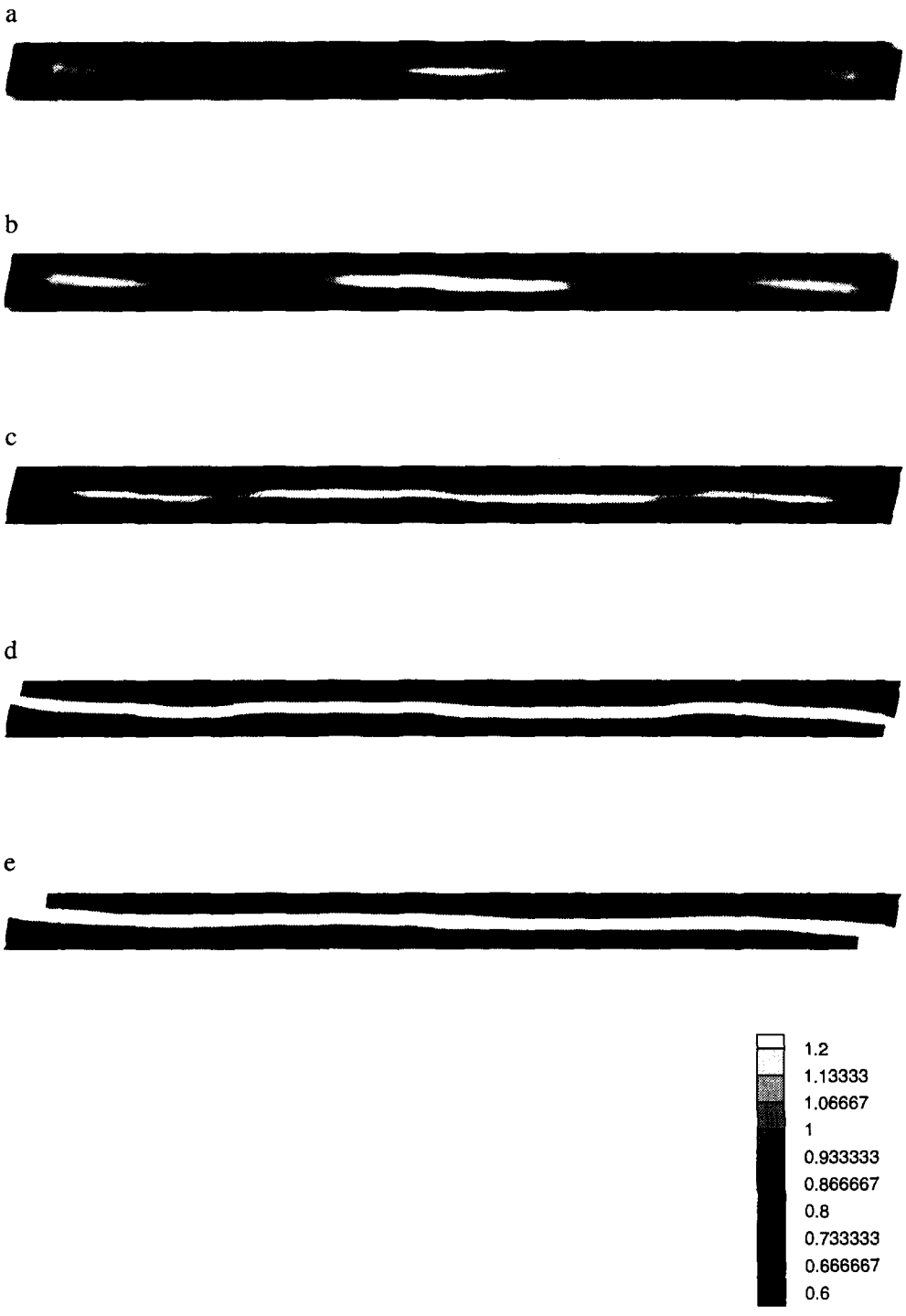


Fig. 10. Contours of normalized plastic shear strain $\gamma^p/\Gamma^p$ for $C^R/s_0 = 0$ at various deformation stages: (a) $\Gamma = 0.16$; (b) $\Gamma = 0.18$; (c) $\Gamma = 0.22$; (d) $\Gamma = 0.34$; (e) $\Gamma = 0.77$.

shear deformation at normalized applied strain-rates $\dot{\Gamma}/\dot{\gamma}_0$ ranging over several orders of magnitude. The increase of the plastic flow stress due to an increase of the strain rate is seen to be small, about 7% for one decade of strain-rate. It seems that the main effect of strain-rate is to shift the shear stress strain curve vertically without changing its shape, while the normal stress is insensitive to the shear rate. The differences in plastic shear strain distributions under different strain-rates are found to be small, so that it is concluded that shear band initiation and propagation are not sensitive to strain-rate within the range considered.

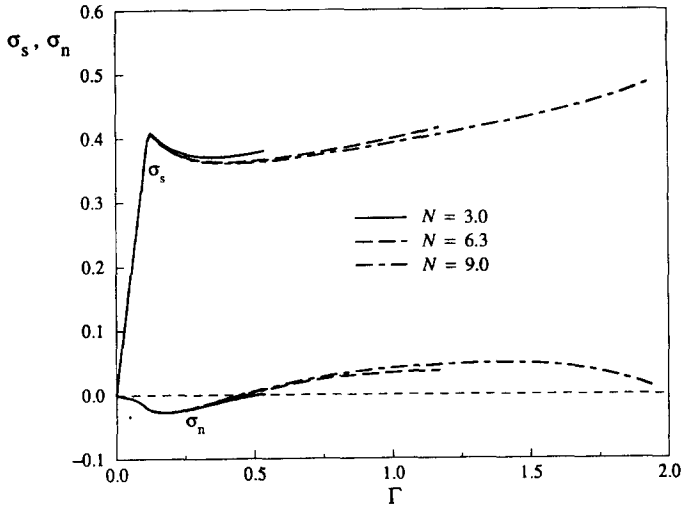


Fig. 11. Influence of the orientation hardening parameter $N$ on the predicted shear and normal stress responses under simple shear for a material with $C^R/s_0 = 0.66$. All other parameters are as in Fig. 2.

### 4.5. *Edge effects*

As mentioned before, the simple shear test carried out by G'Sell and co-workers is a highly inhomogeneous deformation process due to mainly the free edge effects. G'Sell *et al.* (1983) observed that the free edges of the specimen were curved and had a convex (bulging) curvature (see also the profiles of the specimen in Fig. 3). They explained these observations by, on one hand, the constraint effect of the grips which react against the rotational moment imposed by the couple of the shearing forces, and on the other hand by the departure from the ideal simple shear condition in which the ends of the specimen must also carry appropriate tractions, in general normal to and parallel to the end surfaces.

In a preliminary study, Wu and Van der Giessen (1992b) have considered the simple shear of a polycarbonate specimen of infinite length in the shear direction, i.e. $B_0/A_0 \to \infty$. The problem solved (Wu and van der Giessen, 1992b) was effectively a 1-D problem across the width of the slab. In that analysis, the deformation inhomogeneity was reduced substantially because of the absence of free edges. To further assess the edge effects, we also calculated the stress response to homogeneous simple shear to a shear strain $\Gamma$ by direct straightfoward integration of the constitutive equations. The numerical results of these

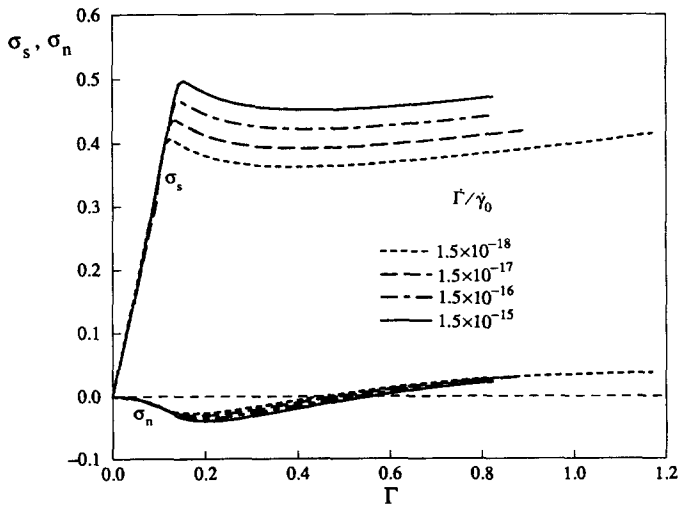


Fig. 12. Influence of the normalized applied strain-rate $\dot{\Gamma}/\dot{\gamma}_0$ on the predicted shear and normal stress responses to simple shear.

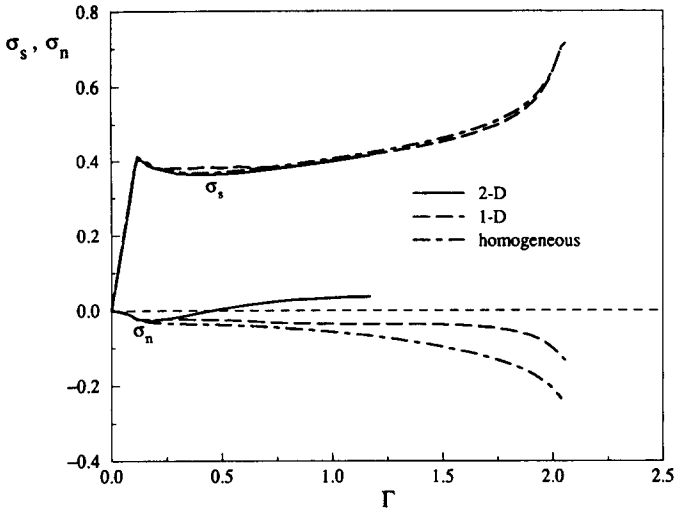


Fig. 13. Predicted shear and normal stress responses to homogeneous, 1-D ($B_0/A_0 \to \infty$) and 2-D ($B_0/A_0 = 15$) simple shear deformations, respectively. The material parameters are as in Fig. 2.

three different cases (referred to as homogeneous, 1-D and 2-D simple shear deformations, respectively) are presented in Fig. 13. Generally, the differences in predicted shear stress are small. This is further substantiated by Fig. 14 which shows the shear and normal stress distributions over the boundary a–b in the specimen (see Fig. 1) in the 2-D analysis at an applied shear strain of 0.6. It is seen that the shear stress distribution is relatively uniform over the boundary. Perhaps the only noteworthy difference in predicted shear stress response is that the 1-D calculation somewhat underestimates the strain softening (see Fig. 13). The reason for this is that in the 1-D analysis we essentially neglect the shear band propagation in the shear direction, while during those stages the shear stress should drop according to the experimental observation (G'Sell and Gopez, 1985). Once the shear band is complete at an applied strain of about 0.80, the shear stress response found in the 2-D case is virtually identical to that in the 1-D case. The very small systematic differences in predicted shear stress between the homogeneous case and the finite element calculations is probably due to the initial imperfection assumed in the latter.

Quite remarkably, the differences seen in Fig. 13 among the three cases in predicted overall normal stress are much larger than in the predicted shear stress. The calculations of all cases give virtually identical predictions of the compressive normal stress for applied

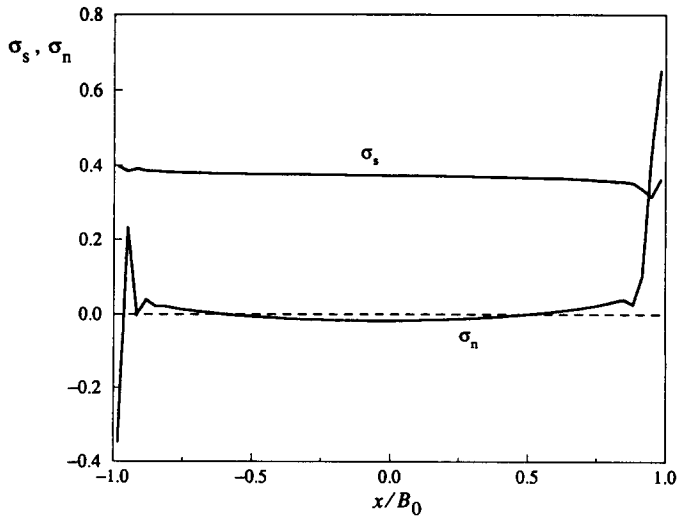


Fig. 14. Shear and normal stress distributions over the boundary a–b of the specimen (see Fig. 1) at an applied shear strain of $\Gamma = 0.6$.

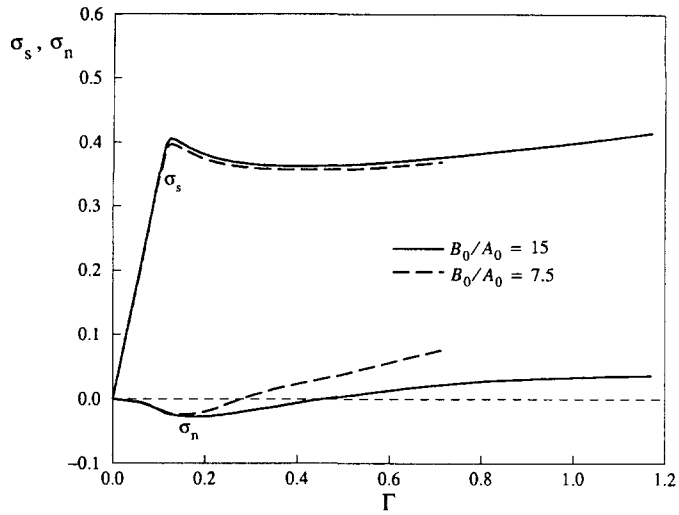


Fig. 15. Influence of the aspect ratio $B_0/A_0$ on the predicted shear and normal stress responses under simple shear.

strains up to $\Gamma = 0.12$. From that point on, the normal stresses in the homogeneous and 1-D cases evolve monotonically and remain compressive, whereas the overall normal stress found in the 2-D analysis becomes tensile eventually. Figure 14 now shows that the predicted normal stresses in the 2-D case along a–b are small and quite uniformly distributed over most of the boundary except at the corners b and a, where high compressive and very high tensile stresses were found, respectively. The resulting average normal stress turns out to be tensile.

Furthermore, G'Sell *et al.* (1983) reported that the perturbation in strain distribution caused by the free edges was significant in end zones of length equal to the width $2A_0$ of the specimen. This means that the edge effects themselves depend on the aspect ratio $B_0/A_0$ and that the larger the value of $B_0/A_0$, the smaller the edge effects. While $B_0/A_0 = 15$ in previous computations, Fig. 15 shows the predicted shear and normal stress responses of a specimen with $B_0/A_0 = 7.5$. In this calculation, we used a regular mesh consisting of $24 \times 60$ elements. It is found that the shear stresses in the thick specimen ($B_0/A_0 = 7.5$) are slightly lower than those in the slender specimen ($B_0/A_0 = 15$); this is probably due to the fact that in all calculations we use the same initial imperfection shape (15), so that the average value of the initial shear strength ($s_0 + \Delta s_0$) in the thick specimen is then slightly smaller than that in the slender specimen. At large strains, the predicted tensile normal stresses in the thick specimen are much higher than those in the narrow specimen. Furthermore, the calculation for the thick specimen stopped at $\Gamma \approx 0.71$ when the maximum plastic stretch approached the locking stretch $\sqrt{N}$ of the network, while for the slender specimen the locking stretch was not reached prior to $\Gamma \approx 1.2$. These observations clearly show that the edge effects increase with the thickness of the specimen. This is consistent with the conclusion of G'Sell *et al.* (1983).

To assess the influence of the geometry on the initiation and propagation of the shear band, Fig. 16 shows contour plots of the normalized plastic shear strain in the thick specimen at various stages of the deformation. Comparing with Fig. 3, it is clear that the velocity of the shear band propagation in the shear direction is much faster in the thick specimen than in the slender specimen. Furthermore, the velocity in the thickness direction is lower in the thick specimen than in the slender specimen. Finally, the plastic strain concentration at the corner a of the thick specimen is much higher than that in the slender specimen.

## 5. AN EXAMPLE FOR POLYCARBONATE

To enable a direct comparison with experimental data for polycarbonate (PC) by Gopez (1983) we have taken the actual dimensions to be the same as in Gopez (1983), i.e.

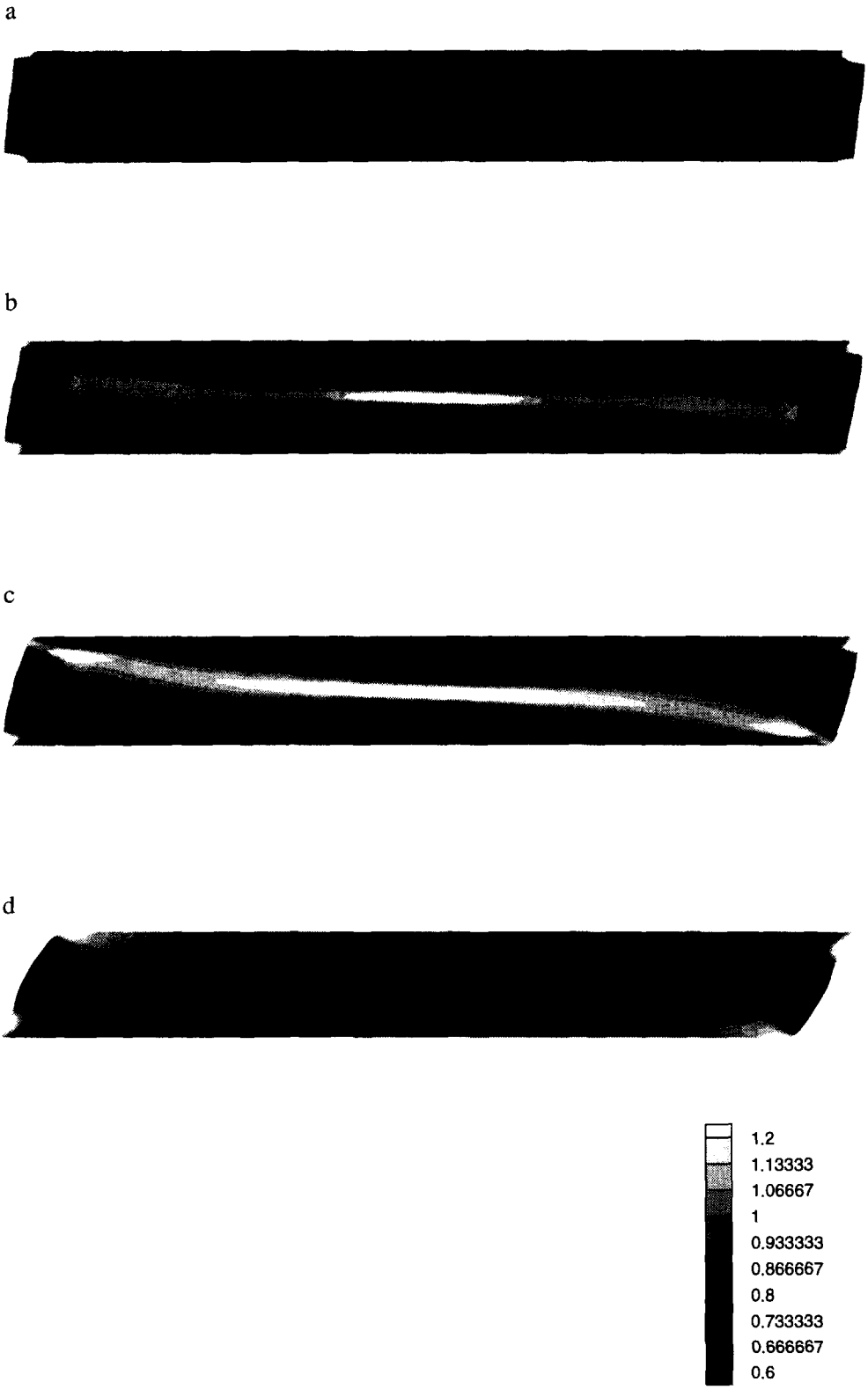


Fig. 16. Contours of normalized plastic shear strain $\gamma^p/\Gamma^p$ for the specimen with $B_0/A_0 = 7.5$ at various deformation stages: (a) $\Gamma = 0.12$, (b) $\Gamma = 0.20$, (c) $\Gamma = 0.30$, (d) $\Gamma = 0.71$. The material parameters are as in Fig. 2.

$2A_0 = 4$ mm and $2B_0 = 60$ mm (see Fig. 1). The opposite faces are displaced at a constant velocity $\dot{U} = 1.2 \times 10^{-5}$ m/s corresponding to an applied shear rate of $\dot{\Gamma} = 3 \times 10^{-3}\ s^{-1}$.

At room temperature ($T = 294$ K), the following values of the parameters that determine the stress-rate, temperature dependence and softening behaviour for PC are used: $\dot{\gamma} = 2 \times 10^{15}\ s^{-1}$, $A = 240$ K/MPa, $s_0 = 97$ MPa, $s_{ss}/s_0 = 0.92$, $h = 500$ MPa and $\alpha = 0.08$, while Young's modulus and Poisson's ratio are taken as $E = 910$ MPa and $\nu = 0.3$, respectively. Most of this data has been taken from the experiment carried out by Boyce and Arruda (1990), but the saturation value $s_{ss}$ has been chosen to fit the softening behaviour observed during large strain plastic torsion of PC by Wu and Turner (1973) (see also Wu and van der Giessen, 1993c), while Young's modulus is chosen smaller than the experimental value of $E = 2300$ MPa for reasons discussed in the previous section. The parameters $C^R$ and $N$ that govern the orientation hardening are taken as $C^R = 5.7$ MPa and $N = 6.3$, which are reasonable compared with experimental values (see Reference 27 in G'Sell, 1986). Admittedly, the material parameters have been compiled from different sources involving different experiments on material that is likely to be not exactly the same, but because of lack of sufficient experimental data this was the best we could do. We shall simply employ these parameters, bearing in mind that the major purpose of this paper is to numerically study the initiation and propagation of shear bands.

Figure 17 shows the predicted stress reponses to plane strain simple shear, along with the experimental data by Gopez (1983). The characteristics of the predictions have already been discussed following Fig. 2, in which the numerical results were presented in terms of the nondimensional shear stress $\sigma_s$ and normal stress $\sigma_n$ defined in (18). The predicted shear stress is in a good agreement with the experimental data, but the predicted normal stress is found to be about 6 times larger in magnitude than the experimental data. For the purpose of a qualitative comparison with the experimental data, the figure also shows the experimental normal stress results multiplied by 7. It is seen that the shape of the predicted normal stress curve is quite unusual but similar to that observed experimentally in polycarbonate (Gopez, 1983). The contour plots of plastic shear strain at various deformation stages have been presented in Fig. 3. The predicted initiation and subsequent propagation of the shear band is found to be in good agreement with experimental observations (G'Sell and Gopez, 1985). Therefore we conclude that the constitutive model, together with the numerical tool used here, is capable of capturing the major characteristics of the large simple shear behaviour in a qualitatively reasonable way.

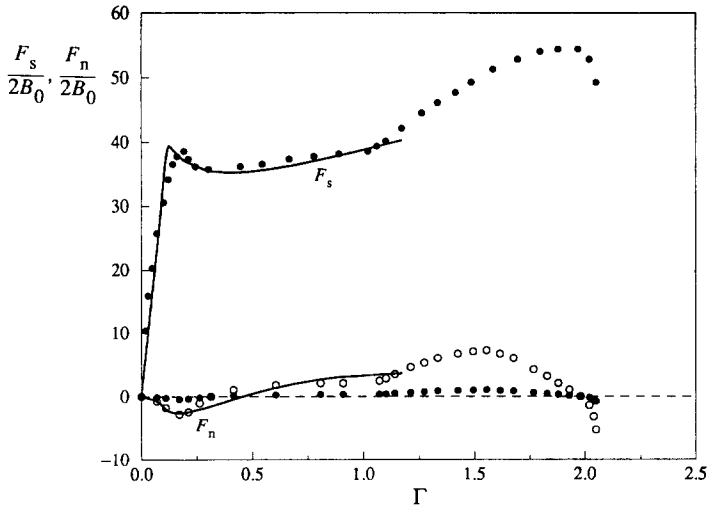


Fig. 17. Predicted overall shear and normal stress response to simple shear for polycarbonate. The dots (●) are experimental data points from Gopez (1983). The open circles (○) are the experimental values for the average normal stress $F_n/(2B_0)$ multiplied by a factor of 7.

## 6. DISCUSSION AND CONCLUSION

In this paper, 2-D finite element analysis has been used to simulate large simple shear tests of amorphous glassy polymers, focussing attention on the initiation and propagation of the shear band. The mesh sensitivity and the effects of initial imperfection, strain softening, orientation hardening, strain-rate as well as the edge effects have been discussed in detail.

The predicted numerical results have been compared with experimental data for polycarbonate, based on material properties taken from independent sources. In general, the agreement is reasonable and the initiation and propagation of shear bands is predicted well. However, a number of features in the experimental results are not picked up by the analysis.

Although the variations of thickness of the specimen are relevant to second-order terms in the strain tensor and may be neglected to a first approximation as suggested by G'Sell (1986), the simple shear test is in fact a 3-D problem. As reported by G'Sell and Gopez (1985), phenomena such as cracking and the drawing of the material from outside the gauge section significantly affect the overall response at large strains. These 3-D effects cannot be taken into account in the 2-D simulation. Therefore, the decrease in hardening slope, due to the microcracking and the drawing-in of material from the grip section at very large strains, is not picked up by the analysis (see Fig. 17). However, a constitutive model for describing the microcracking phenomenon is not available, while full 3-D analyses still impose severe computational requirements. On the other hand, these 3-D effects become critical only at very large strains (G'Sell *et al.*, 1983). Therefore, a proper plane strain type simple shear analysis should be of practical use.

The experiment carried out by Gopez (1983) showed increased hardening in the nominal shear stress–shear strain curve at strains beyond $\Gamma \approx 1.2$ (see Fig. 17). In the homogeneous and 1-D simple shear deformations, the predicted shear stresses go up rapidly when the maximum plastic stretches approach the locking stretch $\sqrt{N}$ of the molecular chain network (see Fig. 13). However, our plane strain type 2-D analysis did not reveal similar effects (see Fig. 13 or Fig. 17). This too is due to the inhomogeneity resulting from the edge effects. Actually, the local shear stress near the free edges does show accelerated hardening when the local maximum plastic stretch approaches $\sqrt{N}$. However, the maximum plastic stretch in locations away from the free edges is still much less than $\sqrt{N}$, so that the resulting average shear stress does not exhibit this enhanced hardening.

We have demonstrated that a sufficiently fine mesh is needed in order to resolve the shear band. In a 3-D simulation of simple shear, Arruda and Boyce (1992) did not observe a shear band at the location of the initial imperfection. It is likely that this is caused by the fact that their mesh, which used only 6 elements in the direction perpendicular to the shear direction, was not fine enough. Our plastic shear strain distributions obtained with a sufficiently fine mesh clearly show the initiation and propagation of the shear band (see Fig. 3 or Fig. 5), which is in good agreement with the experimental observations (G'Sell and Gopez, 1985). However, it is worthwhile to point out that, perhaps unexpectedly, the predicted shear band is not a straight line parallel to the shear direction [see Fig. 3(c) or (d)]. G'Sell and co-workers have not clearly indicated the shape of the shear band in their experimental observations, but the experiments carried out very recently by Meijer and coworkers (1993) at Eindhoven University of Technology strongly support our predicted shear band shapes.

As pointed out by Grenet and G'Sell (1990), an important problem in polymer science is to understand what are the driving factors that control the kinetics of shear band propagation. Our numerical results indicate that there is no evidence of initiation and propagation of a shear band in the limiting case of no intrinsic softening. Thus, it appears that the intrinsic softening is the driving force to promote initiation of the shear band and its propagation in the shear direction. The effects of orientation hardening on initiation and propagation of shear band have also been studied. In the limiting case of no orientation hardening, the fully elongated shear band will localize (see Fig. 10) and the applied strain will concentrate entirely in the band. Therefore we conclude that orientation hardening is the driving force for widening of the shear band.

The secondary normal stress during simple shear is mainly due to the development and subsequent rotation of the induced anisotropy. For the amorphous polymers considered here, this anisotropy is associated with the stretching of the entangled molecular chain structure. It is well-known that the prediction of such second-order phenomena generally shows a rather strong dependence on the constitutive models, in particular the description of anisotropic hardening, and thus provide an effective means for assessing the adequacy of such constitutive models. Although advances in the understanding of second-order effects appear to come primarily from researches on metals (see e.g. Harren *et al.*, 1989; van der Giessen *et al.*, 1992), a number of characteristic aspects in amorphous glassy polymers now begins to be assessed (see e.g. Wu and van der Giessen, 1993a,b,c). Figure 17 shows that although the normal stress predicted with the present constitutive model is much larger than the experimental data, its shape is similar to that observed experimentally. As we mentioned before, the unrealistically large normal stress is likely to be due in part to the high stress concentration at the corners (see Fig. 14). Taking into account the effects of microcracking and the drawing-in of the material from outside the gauge section, which will reduce the stress concentration, and the resulting nominal normal stress will be improved significantly.

We have discussed the effects of initial imperfections in some detail. It was found that, within the strain-range considered, the overall response in terms of nominal shear and normal stresses is not sensitive to the initial imperfection. This supports the approximation involved in previous numerical simulations of the large strain plastic torsion test (Wu and van der Giessen, 1993c); the overall response is only affected slightly by the shear band propagation process. This is particularly convenient when such tests are to be used for the determination of material parameters. It thus seems that the torsion test provides an excellent means for obtaining experimental data for the constitutive behaviour of elastic–plastic solids at large to very large deformations. The major advantage over the simple shear test is that deformations of a solid bar in torsion remain axially homogeneous up to final failure without having to give attention to shear banding (Wu and van der Giessen, 1993c).

Concerning the constitutive aspects, it is noted that we used the affine network theory to model orientational hardening. The idea of using an affine network theory to model the stretching of the molecular network assumes that the junction points in the network remain intact. However, it has been suggested in the literature (see e.g. Raha and Bowden, 1972; Botto *et al.*, 1987) that physical entanglements in amorphous polymers are being pulled out during deformation. In terms of our network model this would mean that the number of chains $n$ reduces in the course of the deformation process, while the number of links $N$ per chain increases, thus reducing the stiffness of the network. This would reduce the predicted normal stress level and at the same time extend the numerical simulation to larger strains by increasing the limit stretch. Furthermore we note that especially the normal stress predicted here may depend sensitively on the particular way of incorporating deformation-induced anisotropy by means of the Mises type effective shear stress concept in (9). This is likely to be rather important in the above simple shear problem, where the stress history is non-proportional and significant rotations of the principal axes occur. A totally different approach to modelling orientational hardening has been adopted by Batterman and Bassani (1990). All these constitutive aspects require further study. The formulation of improved models and their implications are in progress and will be reported elsewhere.

## REFERENCES

Anand, L. (1979). On H. Hencky's approximation strain-energy function for moderate deformation. *J. Appl. Mech.* **46,** 78–82.

Argon, A. S. (1973). A theory for the low-temperature plastic deformation of glassy polymers. *Phil. Mag.* **28,** 839–865.

Arruda, E. M. and Boyce, M. C. (1991). Evolution of plastic anisotropy in amorphous polymers during finite straining. In *Anisotropy and Localization of Plastic Deformation* (Edited by J.-P. Boehler and A. S. Khan), pp. 483–488. Elsevier Applied Science, London.

Arruda, E. M. and Boyce, M. C. (1992). The anisotropy of large deformation in glassy polycarbonate. In *Modelling*

*of Plastic Deformation and its Engineering Applications* (Edited by S. I. Andersen *et al.*), pp. 181–188. Roskilde, Denmark.

Arruda, E. M. and Boyce, M. C. (1993). Evolution of plastic anisotropy in amorphous polymers during finite straining (submitted for publication).

Batterman, S. D. and Bassani, J. L. (1990). Yielding, anisotropy, and deformation processing of polymers. *Polym. Engng Sci.* **30,** 1281–1287.

Botto, P. A., Duckett, R. A. and Ward, I. M. (1987). The yield and thermoelastic properties of oriented poly (methyl methacrylate). *Polymer* **28,** 257–262.

Bowden, P. B. (1973). The yield behaviour of glassy polymers. In *The Physics of Glassy Polymers* (Edited by R. N. Haward), pp. 279–339. Applied Science Publishers, Essex.

Boyce, M. C., Parks, D. M. and Argon, A. S. (1988). Large inelastic deformation of glassy polymers, Part I: rate dependent constitutive model. *Mech. Mater.* **7,** 15–33.

Boyce, M. C. and Arruda, E. M. (1990). An experimental and analytical investigation of the large strain compressive and tensile response of glassy polymers. *Polym. Engng Sci.* **30,** 1288–1298.

Buisson, G. and Ravi-Chandar, K. (1990). On the constitutive behaviour of polycarbonate under large deformation. *Polymer* **31,** 2071–2076.

Gopez, A. J. (1983). *Étude de la Déformation du Polycarbonate en Cisaillement Simple.* Thèse d'Ingenieur, CNAM, Nancy, France.

Grenet, J. and G'Sell, C. (1990). Observation and modelling of shear-band propagation in glassy polycarbonate. *Polymer* **31,** 2057–2065.

G'Sell, C. (1986). Plastic deformation of glassy polymers: Constitutive equations and macromolecular mechanisms. In *Strengths of Metals and Alloys* (Edited by H. J. McQueen *et al.*), pp. 1943–1982. Pergamon Press, Oxford.

G'Sell, C., Boni, S. and Shrivastava, S. (1983). Application of the plane simple shear test for determination of the plastic behaviour of solid polymers at large strains. *J. Mat. Sci.* **18,** 903–918.

G'Sell, C. and Gopez, A. J. (1985). Plastic banding in glassy polycarbonate under plane simple shear. *J. Mat. Sci.* **20,** 3462–3478.

G'Sell, C. and Jonas, J. J. (1979). Determination of the plastic behaviour of solid polymers at constant true strain rate. *J. Mat. Sci.* **14,** 583–591.

Harren, S., Lowe, T. C., Asaro, R. J. and Needleman, A. (1989). Analysis of large-strain shear in rate-dependent face-centered cubic polycrystals: Correlation of micro- and macromechanics. *Proc. R. Soc. Lond.* **328A,** 443–500.

Haward, R. N. (1980). The effect of chain structure on the annealing and deformation behaviour of polymers. *Coll. Poly. Sci.* **258,** 643–661.

Haward, R. N. and Thackray, G. (1968). The use of a mathematical model to describe isothermal stress-strain curves in glassy thermoplastics. *Proc. R. Soc. Lond.* **302A,** 453–472.

Lee, E. H. (1969). Elastic-plastic deformation at finite strains. *J. Appl. Mech.* **36,** 1–6.

Meijer, H. E. H. (1993). Private communication.

Neale, K. W. and Tugcu, P. (1985). Analysis of necking and neck propagation in polymeric materials. *J. Mech. Phys. Solids* **33,** 323–337.

Needleman, A. (1988). Material rate dependence and mesh sensitivity in localization problems. *Comp. Mech. Appl. Mech. Engng* **67,** 69–85.

Needleman, A. and Tvergaard, V. (1984). Finite element analysis of localization in plasticity. In *Finite Elements, Special Problems in Solid Mechanics* (Edited by J. T. Oden and G. F. Carey), Vol. V, pp. 94–157. Prentice-Hall.

Peirce, D., Shih, C. F. and Needleman, A. (1984). A tangent modulus method for rate dependent solids. *Comput. Struct.* **18,** 875–887.

Raha, S. and Bowden, P. B. (1972). Birefringence of plastically deformed poly (methyl methacrylate). *Polymer* **13,** 174–183.

Rice, J. R. (1977). The localization of plastic deformation. In *Theoretical and Applied Mechanics* (Edited by W. T. Koiter), pp. 207–220. North-Holland Publishing Company.

Treloar, L. R. G. and Riding, G. (1979). A non-Gaussian theory for rubber in biaxial strain. I. Mechanical properties. *Proc. R. Soc. Lond.* **369A,** 261–280.

van der Giessen, E. and Neale, K. W. (1993). Analysis of the inverse Swift effect using a rate-sensitive polycrystal model. *Comp. Meth. Appl. Mech. Engng* **103,** 291–313.

van der Giessen, E., Wu, P. D. and Neale, K. W. (1992). On the effect of plastic spin on large strain elastic–plastic torsion of solid bars. *Int. J. Plast.* **8,** 773–801.

Wang, M. C. and Guth, E. (1952). Statistical theory of networks of non-Gaussian flexible chains. *J. Chem. Phys.* **20,** 1144–1157.

Wu, P. D. and van der Giessen, E. (1992a). On improved 3-D non-Gaussian network models for rubber elasticity. *Mech. Res. Comm.* **19,** 427–433.

Wu, P. D. and van der Giessen, E. (1992b). A modified 3-D constitutive model for glassy polymers and its application to large simple shear of polycarbonate. In *Modelling of Plastic Deformation and its Engineering Applications* (Edited by S. I. Andersen *et al.*), pp. 519–524. Roskilde, Denmark.

Wu, P. D. and van der Giessen, E. (1993a). On improved network models for rubber elasticity and their applications to orientation hardening in glassy polymers. *J. Mech. Phys. Solids* **41,** 427–456.

Wu. P. D. and van der Giessen, E. (1993b). Large strain visco-plastic torsion of circular bars of glassy polymers. In *Advances in Engineering Plasticity and its Applications* (Edited by W. B. Lee), pp. 477–484. Elsevier Science Publishers B.V., Amsterdam.

Wu, P. D. and van der Giessen, E. (1993c). On large strain inelastic torsion of glassy polymers. *Int. J. Mech. Sci.* **35,** 935–951.

Wu, W. and Turner, A. P. L. (1973). Shear bands in polycarbonate. *J. Polym. Sci. Polym. Phys. Edition* **11,** 2199–2208.

Zbib, H. M., Shawki, T. G. and Batra, R. C. (eds) (1992). Material instabilities. *Appl. Mech. Rev.* **45**(3), part 2.